Journal of Biomedical Optics 9(6), 1187–1197 (November/December 2004)

Raman microspectroscopic mapping studies of human bronchial tissue

Senada Koljenović
Tom C. Bakker Schut
Erasmus Medical Center Rotterdam
Department of General Surgery
Laboratory of Intensive Care Research
and Optical Spectroscopy
Rotterdam, The Netherlands

Jan P. van Meerbeeck
Erasmus Medical Center Rotterdam
Department of Lung Diseases
Rotterdam, The Netherlands
and
University Hospital Ghent
Thoracic Oncology
Ghent, Belgium

Alexander P. W. M. Maat
Erasmus Medical Center Rotterdam
Department of Cardiothoracic Surgery
Rotterdam, The Netherlands

Sjaak A. Burgers
Erasmus Medical Center Rotterdam
Department of Lung Diseases
Rotterdam, The Netherlands
and
Antoni van Leeuwenhoek Hospital
Netherlands Cancer Institute
Amsterdam, The Netherlands

Pieter E. Zondervan
Johan M. Kros
Erasmus Medical Center Rotterdam
Department of Pathology
Dr. Molewaterplein 40
3015 GD, Rotterdam
The Netherlands

Gerwin J. Puppels
Erasmus Medical Center Rotterdam
Department of General Surgery
Laboratory of Intensive Care Research
and Optical Spectroscopy
Dr. Molewaterplein 50
3015 GE, Rotterdam
The Netherlands
E-mail: g.puppels@erasmusmc.nl

Abstract. Characterization of the biochemical composition of normal bronchial tissue is a prerequisite for understanding the biochemical changes that accompany histological changes during lung cancer development. In this study, 12 Raman microspectroscopic mapping experiments are performed on frozen sections of normal bronchial tissue. Pseudocolor Raman images are constructed using principal component analysis and K-means cluster analysis. Subsequent comparison of Raman images with histologic evaluation of stained sections enables the identification of the morphologic origin (e.g., bronchial mucus, epithelium, fibrocollagenous stroma, smooth muscle, glandular tissue, and cartilage) of the spectral features. Raman spectra collected from the basal side of epithelium consistently show higher DNA contributions and lower lipid contributions when compared with superficial epithelium spectra. Spectra of bronchial mucus reveal a strong signal contribution of lipids, predominantly triolein. These spectra are almost identical to the spectra obtained from submucosal glands, which suggests that the bronchial mucus is mainly composed of gland secretions. Different parts of fibrocollagenous tissue are distinguished by differences in spectral contributions from collagen and actin/myosin. Cartilage is identified by spectral contributions of glycosaminoglycans and collagen. As demonstrated here, *in situ* analysis of the molecular composition of histologic structures by Raman microspectroscopic mapping creates powerful opportunities for increasing our fundamental understanding of tissue organization and function. Moreover, it provides a firm basis for further *in vitro* and *in vivo* investigations of the biochemical changes that accompany pathologic transformation of tissue.
[DOI: 10.1117/1.1805555]

Keywords: Raman mapping; bronchial tissue; epithelium; glands; secretions; cartilage.

Paper 03146 received Dec. 4, 2003; revised manuscript received Mar. 16, 2004; accepted for publication Mar. 16, 2004.

1 Introduction

The prognosis for patients with lung cancer essentially depends on the stage of the disease at the time of diagnosis. Because of this, there has been a shift in diagnostic and therapeutic standards from a focus on cancer that presents itself clinically, toward premalignant lesions [i.e., dysplasia and carcinoma *in situ* (CIS)]. A number of optical techniques are being evaluated as tools for detection of premalignant bronchial tissue. Different studies have reported that laser-induced fluorescence endoscopy (LIFE), when used as an adjunct to standard white light bronchoscopy (WLB), resulted in higher overall sensitivity for detecting dysplasia and CIS when compared with WLB alone.[1–5] However, this improvement in sensitivity is associated with a statistically significant decrease in specificity.[5] Hence, there is a need for additional tools that can detect premalignant epithelial changes with higher sensitivity and specificity, and therefore could facilitate the treatment of lung cancer. To make it possible to detect biochemical alterations that accompany the development of lung cancer, knowledge about the biochemical composition of different

Address all correspondence to Gerwin J. Puppels, Erasmus Univ/Rotterdam, Univ Hospital Surgery 10 M, Dr. Molewaterplein 40, Rotterdam NL-3015 GD, Netherlands. Tel:31-0-4087671; Fax: 31-10-4087671; E-mail: puppels@riverd.com

1083-3668/2004/$15.00 © 2004 SPIE

structures in normal lung tissue is essential. Raman spectroscopy provides information about the molecular composition, molecular structures, and molecular interactions in tissue,[6–9] but so far this technique has not been used to study bronchial epithelium.

Raman spectroscopy is a nondestructive optical technique, based on inelastic scattering of light by the molecules in a sample. Since different types of tissue will vary in their overall molecular composition, their Raman spectra will also be different, and can therefore be used as tissue-specific spectroscopic fingerprints. Pathologic changes in molecular composition or structure are reflected in the spectra, enabling development of diagnostic tools based on Raman spectroscopy. Application of Raman spectroscopy as a nondestructive technique for *ex vivo* and *in vivo* tissue characterization (e.g., normal, precancerous, cancerous tissues) has shown significant progress in recent years.[6–16] Miniaturization of flexible fiber optic probes that are suitable for Raman spectroscopy is opening new pathways toward *in vivo* clinical applications, e.g., in cardiology and oncology.[15,16] A complicating factor is heterogeneous structure and chemical composition of tissues. For a thorough understanding of tissue Raman signals, it is necessary to analyze the contribution of different structures in the tissue to the overall Raman signal. *In vitro* Raman microspectroscopic mapping studies of thin tissue sections provides a clear insight into this matter and allows an *in situ* biochemical analysis at a micron scale. So far, only one study[14] on lung tissue using Raman spectroscopy has been reported. However, that study, which addressed the feasibility of measuring *in vivo* Raman spectra without fluorescence background using 1064-nm excitation and a newly developed InP/InGaAsP multichannel detector, did not focus on a detailed characterization of the chemical composition of normal lung tissue.

We report on the use of Raman microspectroscopic mapping experiments and hematoxilin and eosin (HE) staining of unfixed thin sections of normal human bronchial tissue, to identify tissue regions with different chemical composition and to relate these regions to tissue morphology. This investigation serves as a starting point for a study of malignant transformation of bronchial epithelium, and furthermore, sheds light on the issue of composition and origin of the bronchial mucus.

2 Materials and Methods

2.1 *Sample Handling*

The tissue specimens that were used in this study originated from resection material obtained during surgical procedures at the Department of Cardiothoracic Surgery of the Erasmus MC Rotterdam. After excision, tissue samples were snap frozen by immersion in liquid nitrogen and kept at −80 °C until further use. For sectioning, these frozen samples were mounted on the cryotome stage using Tissue Tek®. Care was taken to only embed the side of the sample needed for mounting to avoid contamination of the rest of the specimen by Tissue Tek®. Mounted samples were cut into 20-μm-thick sections and placed onto calcium fluoride (CaF_2) microscope slides. The passively dried, unfixed tissue sections were used without further treatment. To confirm whether tissue was normal and to identify different structures within the bronchial wall, 5-μm-thick adjacent sections were cut before cutting 20-μm sections. Adjacent sections were stained with HE and histopathologically evaluated. Bright-field images of the unstained tissue sections revealed heterogeneity in tissue structure, which could be linked to the structural heterogeneity observed in the stained adjacent sections. This assessment was used to select regions for Raman mapping. To provide a direct comparison of the Raman mapping results with histology, the 20-μm tissue sections were HE stained as well, after Raman mapping measurements were completed. To confirm whether the tissue morphology was consistent over the thickness, comparison with adjacent sections was performed for all 20-μm sections after they have been microscopically scanned and HE stained. In this study, a total of 12 Raman mapping sessions were performed on ten unstained cryosections of normal bronchial tissue derived from eight patients.

The Medical Ethics Review Board of the Erasmus MC approved the study, and written informed consent was obtained from each patient.

2.2 *Reference Spectra*

Reference Raman spectra were obtained of triolein, deoxyribonucleic acid (DNA), collagen type 1, actin, and tryptophan (Sigma-Aldrich Chemie, Zwijndrecht, The Netherlands). These compounds were used without further purification. DNA (from calf thymus) was dissolved in demineralized water (20 mg/ml). In addition, we also recorded the spectra of the tissue embedding agent used in this study (Tissue Tek®).

2.3 *Raman Microspectrometer*

A near-infrared multichannel Raman microspectrometer, built in-house, was used to collect the Raman spectra of tissue sections. This Raman system was recently described in detail.[17] Briefly, laser light of 847 nm was focused on the sample by an 80× objective, optimized for use in the near-infrared (NIR) spectral region (MIR-plan 80×/0.75, Olympus, Japan). Raman signal was collected in the spectral interval from 400 to 1800 cm^{-1}, with a spectral resolution of 8 cm^{-1}.

Automatic scanning of unstained cryosections (20 μm) of bronchus tissue was enabled by an xyz-motorized, computer-controlled sample stage (Leica DM STC, Cambridge, UK). The laser light was focused below the surface of the tissue at such a depth that the signal intensity was maximized. For each Raman mapping experiment, the tissue area and the scanning step size were selected. Thereby the area of interest was divided up into small square areas (hereafter termed Raman pixel). Spectra were obtained consecutively from the tissue in each of these Raman pixels with a resolution that varied between 1 and 12 μm in different experiments. The 80× microscope objective focused the laser light to a spot of less than 1 μm^2. To obtain a spectrum that is representative of the tissue in a Raman pixel, the area of the Raman pixel was scanned during each spectral measurement. Tissue samples were excited with 90 to 110 mW of laser power during Raman experiments. Spectra were obtained using 10 s of signal collection time per Raman pixel.

Acquisition of Raman spectra and microscopic stage movement was controlled by the WiRE 1.2 software (Renishaw) running under Grams/32 Spectral Notebase Software

(Galactic Industries Corporation, Salem, New Hampshire). Raman mapping software was implemented in Array Basic (the internal software platform of Grams) and controlled the Leica microscope unit and the microscope stage.

2.4 *Data Analysis*

2.4.1 *Pretreatment of spectra*

Following data acquisition, the spectra were first calibrated and corrected for the wavelength-dependent signal detection efficiency of the Raman setup, as described earlier.[18] Interfering background Raman signals originating in the optical elements in the laser light delivery pathway and the CaF_2 slide measured separately were subtracted from the tissue Raman spectra.

2.4.2 *Raman maps*

Pseudocolor Raman maps were constructed from the spectral dataset using multivariate statistical techniques. The first derivative of the spectra was calculated (using the Savitzky-Golay method with a smoothing window of nine points) and the resulting spectra were subsequently scaled so that all the derivative spectra of a map had zero mean and unit standard deviation (autoscaling or standard normal variate scaling).[18] In this way, the influence of any slowly varying fluorescence or background scatter in the spectra, which is noninformative, was minimized.

To orthogonalize and reduce the number of parameters needed to represent the signal variance in the spectral dataset, principal component analysis (PCA)[19] was used. PCA finds the orthogonal directions in spectral space (principal components or PCs) that describe the major sources of spectral variance. The first PC reflects the average spectrum: each subsequent PC is orthogonal to the former and describes a continuously decreasing part of the total variance in the dataset. These PCs are then used as new coordinates, and all spectra in the dataset are expressed as scores on these new coordinates (PCA scores). The scores on the first PCs, together accounting for 99.9% of the variance captured, served as input for K-means cluster analysis (KCA).[20] Cluster analysis was performed to find groups of spectra that have resembling spectral characteristics. KCA was used here because it can easily handle the large amounts of data obtained during Raman mapping experiments.

KCA divides the dataset in a predetermined number of clusters by the following procedure (with N being the number of clusters). First, N spectra are chosen at random from the dataset. These spectra are taken as initial cluster centers. Then the distance of all spectra to these cluster centers is calculated, and the spectra are assigned to the nearest cluster (center). Then for each cluster, a new center is calculated, being the average of all spectra assigned to that cluster. This procedure is repeated until a stable solution is reached. This procedure has recently been used and described in several *in vitro* Raman studies.[11,12]

A Raman spectrum presents the overall molecular composition of the measurement volume in the tissue, because all molecules in the measurement volume contribute to the Raman signal. Spectra that are highly similar, and therefore were obtained from tissue areas of very similar molecular composition, end up in the same clusters. The cluster-membership information was plotted as a pseudocolor map by assigning a color to each cluster. The location of differently colored areas in the pseudocolor Raman maps was compared with the HE-stained tissue section.

Depending on the size of the selected area and mapping resolution, the number of pixels per Raman map varied from 50 to 900 pixels for five Raman maps of small areas within different bronchial structures (mapped with 1-μm resolution) and from 1620 to 12544 pixels in seven experiments, where larger tissue regions were mapped (with 4.4- to 12-μm resolution), comprising epithelium and submucosa.

2.4.3 *Raman difference spectra*

Information about differences in biochemical composition of the various tissue structures can be obtained from positive difference spectra, which are calculated by scaled subtraction of the cluster averages from each other in such a way that the difference spectrum does not show negative Raman features.

2.4.4 *Spectral modeling*

A routine least-squares fitting procedure was performed to obtain information about the differences in chemical composition between various histologic structures. The Raman spectra of individual histologic features were fitted with the spectra obtained from surrounding tissue plus the reference spectra of one or more compounds (i.e., collagen, actin, triolein, and DNA). This (nonrestricted) fitting procedure resulted in positive or negative fit contributions of the reference spectra that point out higher or lower concentrations of the corresponding compounds in tissue structures that were compared. Relative scattering cross sections were not determined, and therefore all fit contributions are presented as arbitrary units and not as weight percentages.

3 Results

To provide an impression of the normal bronchial histology, standard paraffin sections (HE stained) were prepared. Photographs are displayed in Fig. 1. Figure 1(**A**) shows the basic structure of the bronchial wall segment that comprises a ciliated columnar epithelium (indicated E) with underlying lamina propria (indicated Lp, pointed with arrow) and subepithelial tissue termed submucosa (indicated S). The pseudostratified bronchial epithelium [Fig. 1(**B**)] is made up of several cell types with the nuclei at the different heights within the epithelium. Bronchial epithelium is coated by a liquid layer termed bronchial mucus, which plays an important role in the defense of the respiratory tract from inhaled airborne particles that are trapped in this epithelial lining and constantly cleared by the action of ciliary epithelial cells. Due to the staining procedure, bronchial mucus is mostly washed away and therefore visible as a discontinuous epithelial coat in Figs. 1(**A**) and 1(**B**). The submucosa contains variable amounts of smooth muscle (indicated Sm), a partial cartilaginous ring (indicated C) and fibrocollagenous stroma with variable quantities of glands (indicated G) and gland ducts (indicated Gd). The bronchial glands are of the seromucous type and have a branched architecture with secretory cells arranged in islands termed acini. These glands are located superficially and deeply in the submucosa between and beneath cartilaginous plates. They empty into the bronchial lumen through short or

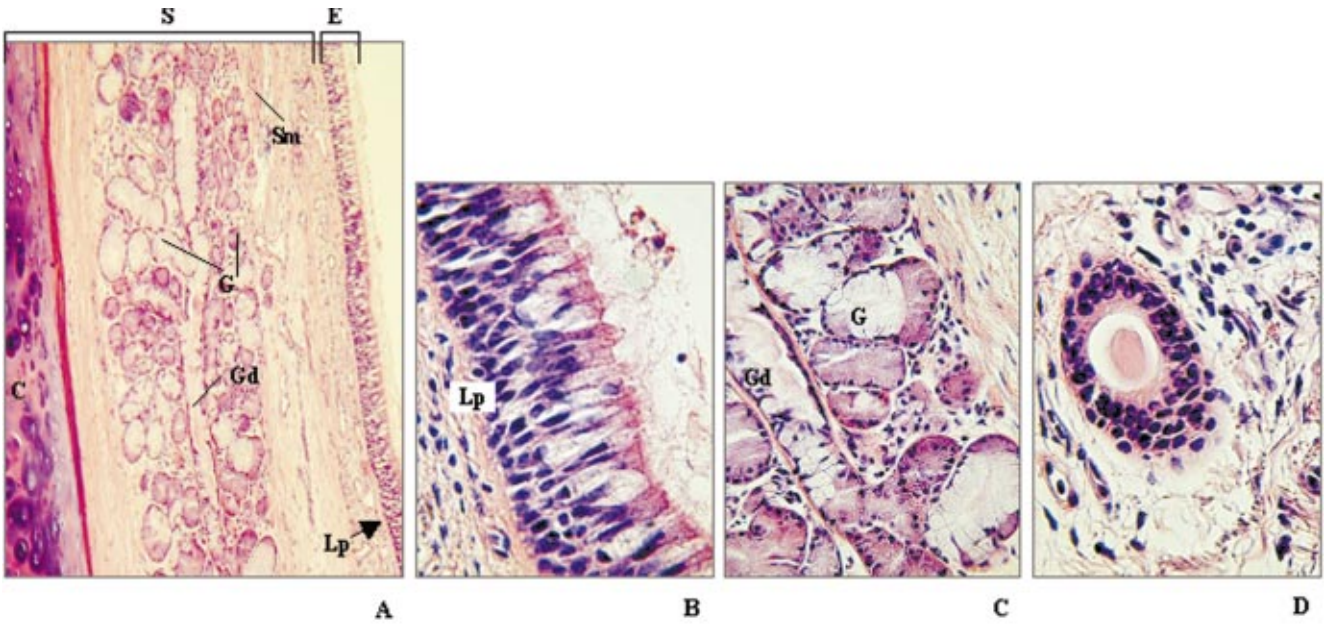

Fig. 1 (**A**) Micrograph (original magnification, ×10) of a HE-stained section showing a transversally cut bronchial wall segment with the pseudostratified columnar ciliated epithelium (indicated E), underlying lamina propria (indicated Lp, pointed by arrow), and submucosa (indicated S). Note the seromucous glands (indicated G), band of smooth muscle (indicated Sm), a large, longitudinally cut, excretory gland duct (indicated Gd), and a part of cartilage plate (indicated C), in submucosa. (**B**), (**C**), and (**D**). Micrographs showing (original magnification, ×60) the histological structure of bronchial wall in more detail. (**B**) Within the epithelium it is evident that the most of the nuclei are located at the basal side. Lamina propria (Lp) is also visible. Bronchial mucus is mostly washed away and therefore visible as a discontinuous epithelial coat. (**C**) Seromucous glands (G) with the (main) excretory duct (Gd). (**D**) Excretory gland duct at a transversal cut with surrounding fibrocollagenous stroma. (Note pink-stained bronchial secretion in the lumen of gland duct.)

Fig. 2 (Following page) Raman microspectroscopic mapping experiments. ($\mathbf{A_1}$) Microphotograph of an unstained section of bronchial wall. Note the presence of a hair-like structure (asterisk, Tissue Tek® artifact) and the liquid layer lining the epithelium (triangle). ($\mathbf{B_1}$) A gross overview Raman map based on KCA using 16 clusters. Spectra (4248) were obtained at a resolution of 6 μm and each spectrum is represented by one pixel. Cluster 1 consists of the spectra obtained at the edge of the tissue section where no tissue was present. A hair-like structure and bronchial mucus (i.e., the liquid layer lining the epithelium) are represented by clusters 2 and 3, respectively. Clusters 4 and 5 correspond with the pseudostratified bronchial epithelium. The superficial part of epithelium, consisting of cytoplasmic components, is represented by cluster 4, cluster 5 represents the basal part that is nuclei rich. Clusters 7 and 15 coincide with submucosal fibrocollagenous stroma tissue, and cluster 8 coincides with a band of smooth muscle (due to loss of tissue during staining procedure not well preserved in HE section). Cluster 9 represents the fibrocollagenous tissue surrounding a transversally cut gland duct. Furthermore, there is a good correspondence of glandular tissue (i.e., seromucous glands and their ducts) with clusters 4, 10, 12, 14, and 16. Note that cluster 3 indicates both the bronchial mucus lining the epithelium and the secretions within the lumen of gland ducts. ($\mathbf{C_1}$) HE stain of the same tissue section showing a segment of the bronchial wall with epithelium (E) and underlying submucosal tissue. Due to the staining procedure, bronchial mucus and gland secretions were washed away. ($\mathbf{A_2}$) Unstained bronchial tissue section containing numerous glands (indicated G) and a partial cartilage (indicated C). ($\mathbf{B_2}$) A pseudocolor map (480 spectra, 8-μm resolution) based on KCA using 13 clusters. The secretory glands (main clusters 6 and 7), fibrocollagenous stroma (clusters 4, 5, 9, and 10), and the cartilage tissue (clusters 12 and 13) are clearly distinguishable and can be easily relocated in the HE-stained section. ($\mathbf{C_2}$) HE staining of the same tissue section showing secretory glands (G) and slightly blue stained cartilage (C). The gland secretions were washed out after HE procedure, as shown in Fig. 1(**C**). ($\mathbf{A_3}$) Unstained section of an area consisting of a part of the bronchial epithelium and a part of the submucosa. ($\mathbf{B_3}$) Raman spectra (4598), obtained at a 4.4-μm resolution, were analyzed by KCA using 11 clusters resulting in a pseudocolor map. At this higher resolution, the basal epithelial side is captured by several clusters (clusters 1 to 5), indicating small areas with higher/lower nuclear contents. Cluster 6 coincides with the luminal epithelial side. ($\mathbf{C_3}$) HE-stained section with the clearly visible lamina propria (Lp) that separates bronchial epithelium from underlying submucosal tissue.

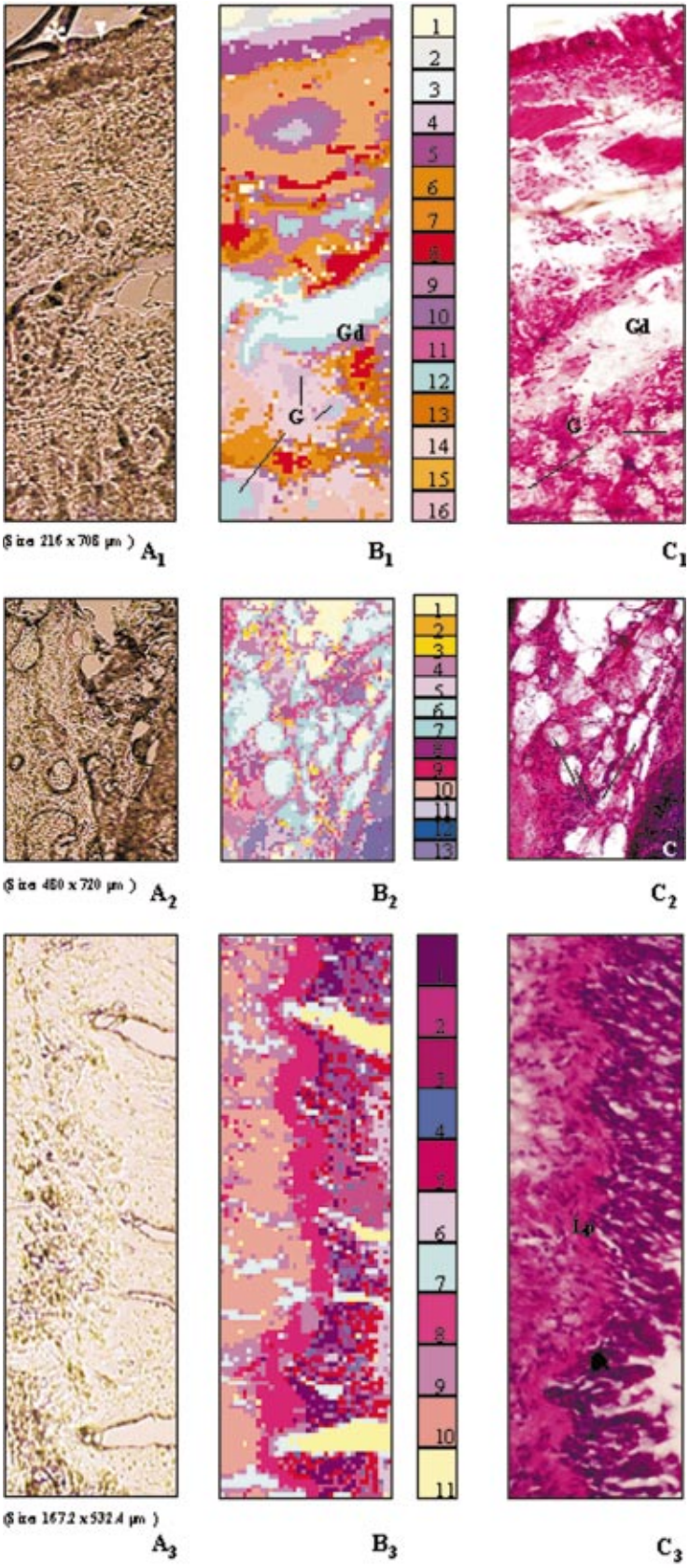
1
2
3
4
5
6
7
8
9
10
11
12
13
14
15
16
Gd
C
Gd
C
(Size 216 x 706 μm) A1
B1
C1
1
2
3
4
5
6
7
8
9
10
11
12
13
C
(Size 480 x 720 μm) A2
B2
C2
1
2
3
4
5
6
7
8
9
10
11
Lp
(Size 1672 x 532.4 μm)
A3
B3
C3

long ducts, depending on their location in the bronchial wall. Glands and gland ducts are shown in more detail in Fig. 1(**C**) and a transversally cut gland duct is shown in the medium-power micrograph in Fig. 1(**D**).

3.1 *Pseudocolor Raman Maps*

The results of three Raman mapping experiments, which are representative of the 12 mapping experiments that were carried out, are shown in Fig. 2. After scanning of the unstained tissue sections [Figs. 2(**A$_1$**), 2(**A$_2$**), and 2(**A$_3$**)], the acquired Raman spectra were analyzed by principal component analysis (PCA) followed by K-means cluster analysis (KCA). This procedure groups similar spectra in one cluster. Each cluster was assigned a color resulting in a pseudocolor Raman map [Figs. 2(**B$_1$**), 2(**B$_2$**), and 2(**B$_3$**)]. The HE staining caused some loss and displacement of tissue, but the overall morphologic aspect of the bronchial wall was preserved [Figs. 2(**C$_1$**), 2(**C$_2$**), and 2(**C$_3$**)]. Comparison of these HE-stained sections with corresponding adjacent sections revealed that in all sections measured, the tissue morphology was consistent over the thickness of 20 μm. This implies that the morphological origin of the spectra that were recorded was well defined. In Fig. 2(**B$_1$**), a Raman map with a pixel size of 6×6 μm is displayed. A comparison of this pseudocolor map with the images of the unstained [Fig. 2(**A$_1$**)] and the HE-stained [Fig. 2 (**C$_1$**)] tissue section shows that different colors in the Raman map correspond with distinct histologic features in the bronchial epithelium and submucosal tissue. The hair-like structure (asterisk) and the bronchial mucus lining the epithelium (triangle) that are visible in the unstained section clearly coincide with clusters 2 and 3 of the Raman map. Such hair-like structures were frequently observed in the unstained sections, but were washed away together with the bronchial mucus during the standard HE-staining procedure and proved to be artifacts. The Raman spectra of this structure (not shown) contain signal contributions of both the medium in which the tissue was embedded before sectioning (Tissue Tek®, spectrum shown later) and of the bronchial mucus. The bronchial epithelium is divided up into two clusters in the pseudocolor Raman map. Cluster 4 coincides with the superficial part, and cluster 5 with the basal part of epithelium. This division reflects the fact that the nuclei are predominantly located on the basal side of the epithelium. Therefore cluster 5 will be referred to as the nuclear epithelial cluster and cluster 4 will be referred to as the cytoplasmic epithelial cluster. The fibrocollagenous stroma tissue (clusters 7 and 15) and smooth muscle (cluster 8) are clearly distinguished from glands and their excretory ducts (clusters 4, 10, 12, 14, 16). It is evident that the luminal content (i.e., gland secretions) of large gland ducts [indicated Gd in Fig. 2(**B$_1$**)] coincides with cluster 3 associated with the bronchial mucus at the epithelial surface. Due to the staining procedure that washes away the secretory contents from glands and their ducts, these structures appear empty in the HE-stained section, as shown in Fig. 2(**C$_1$**).

Figures 2(**A$_2$**), 2(**B$_2$**), and 2(**C$_2$**) show a region with numerous glands and cartilage [Fig. 2(**A$_1$**)] scanned with 8-μm resolution. Again the gland secretions were washed out after routine staining. The Raman map [Fig. 2(**B$_2$**)] and HE section [Fig. 2(**C$_2$**)] correspond well. Clusters 6 and 7 in the Raman map represent the inner parts of most glands. Cartilage tissue [indicated C in Fig. 2(**C$_2$**)] is captured by clusters 12 and 13 in the Raman map.

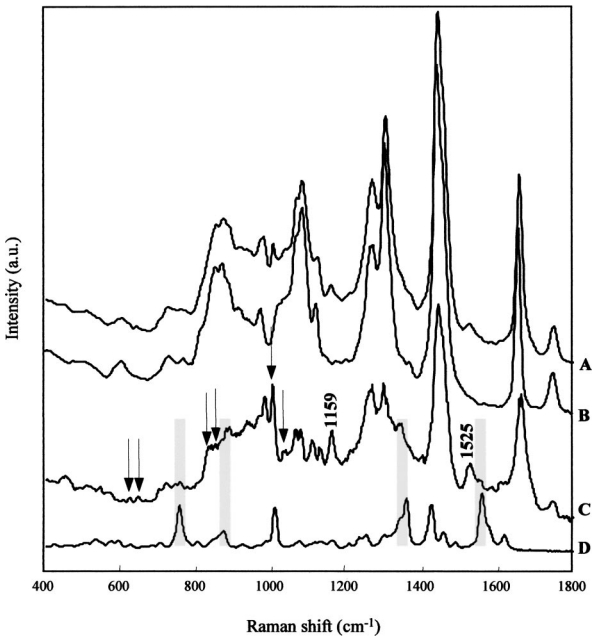

Fig. 3 Raman spectrum of bronchial mucus. A: cluster-average spectrum obtained from bronchial mucus (BM) at the epithelial surface from the unstained tissue section as shown in Fig. 2(**A$_1$**) [cluster 3 in Fig. 2(**B$_1$**)]. B: Raman spectrum of pure triolein shows a striking correspondence with BM spectrum. C: difference spectrum BM minus triolein. The Raman peaks at ~1159 and ~1525 cm^{-1} suggest the presence of carotenoids. Spectral contribution from proteins is suggested by peaks assigned to phenylalanine (at 623, 1002, and 1031 cm^{-1}) and tyrosine (at 643, 833, and 849 cm^{-1}), indicated by arrows. Comparison with the Raman spectrum of pure tryptophan (D) reveals that, although the presence of tryptophan signal contributions cannot be completely excluded (gray bars), there is no clear evidence of the lysozyme presence in the difference spectrum.

A more detailed Raman map of bronchial epithelium [Fig. 2(**B$_3$**)] was obtained at a resolution of 4.4 μm. As is evident from the HE-stained section [Fig. 2(**C$_3$**)], epithelium is separated from submucosa by a clearly visible lamina propria indicated by cluster 8. Also in this Raman map, there is a clear division between the luminal side of the epithelial cells (cluster 6) and the basal side of the epithelial cells, which at this higher resolution is captured in several clusters (clusters 1 to 5).

3.2 *Spectral Analysis*

3.2.1 *Bronchial mucus*

The average spectrum obtained from bronchial mucus at the epithelial surface is displayed in Fig. 3 spectrum A [cluster 3 in Fig. 2(**B$_1$**)]. Comparison with a spectrum of pure triolein (Fig. 3 spectrum B) reveals a strong overlap. The difference of the spectra of bronchial mucus and triolein (Fig. 3 spectrum C) reveals peaks at ~1159 and ~1525 cm^{-1}, which suggests the presence of carotenoids[21] in bronchial mucus. These carotenoid signal contributions were found in tissue samples from four patients. The phenylalanine peaks at 623, 1002, and 1031 cm^{-1} and tyrosine peaks at 643, 833, and 849 cm^{-1} were observed in the tissue specimens of all patients.

This suggests that there is a slight contribution of proteins in the spectra of bronchial mucus. Lysozyme is an important antibacterial constituent of bronchial secretions.[22–24] The Raman spectrum of lysozyme is characterized by strong signal contributions of tryptophan (Fig. 3 spectrum D).[25] For comparison we have obtained the Raman spectrum of pure tryptophan. This shows that, although the presence of tryptophan signal contributions cannot be completely excluded (Fig. 3, gray bars), the difference spectrum does not provide clear evidence of the presence of lysozyme.

3.2.2 *Epithelium*

As illustrated by Figs. 1 and 2, the pseudostratified bronchial epithelium consists of a single layer of cells with most of the nuclei located on the basal epithelial side. The averaged spectra of the nuclear epithelial cluster [cluster 1 in Fig. 2($\mathbf{B_3}$)] and the cytoplasmic epithelial cluster [cluster 6 in Fig. 2($\mathbf{B_3}$)] are shown in Fig. 4 (spectra A and B, respectively). To investigate the underlying differences in molecular composition, a difference spectrum (spectrum C) between these two cluster averages was calculated (nuclear epithelial cluster minus cytoplasmic epithelial cluster). The difference spectrum reveals prominent Raman peaks at 501, 727, 784, 1096, and 1576 cm^{-1}, which can be assigned to DNA (spectrum D, gray bars). As expected, the nuclear epithelial cluster contains a higher DNA concentration than the cytoplasmic epithelial cluster. In the same way, the nuclear epithelial cluster was subtracted from the cytoplasmic epithelial cluster, resulting in the difference spectrum shown in Fig. 4 spectrum E. The strong bands at 1262 and 1305 cm^{-1} are most likely due to fatty acid signal contributions and therefore are probably indicative of a higher concentration of lipids in the cytoplasmic epithelial cluster. A higher protein concentration in this cluster can be deduced from the presence of protein small peaks assigned to phenylalanine (621, 1004, and 1033 cm^{-1}) and tyrosine (644, 831, and 852 cm^{-1}). Furthermore, the Raman bands in the 1546 to 1583 cm^{-1} region are indicative of the presence of hemeproteins[15] such as catalase.[24]

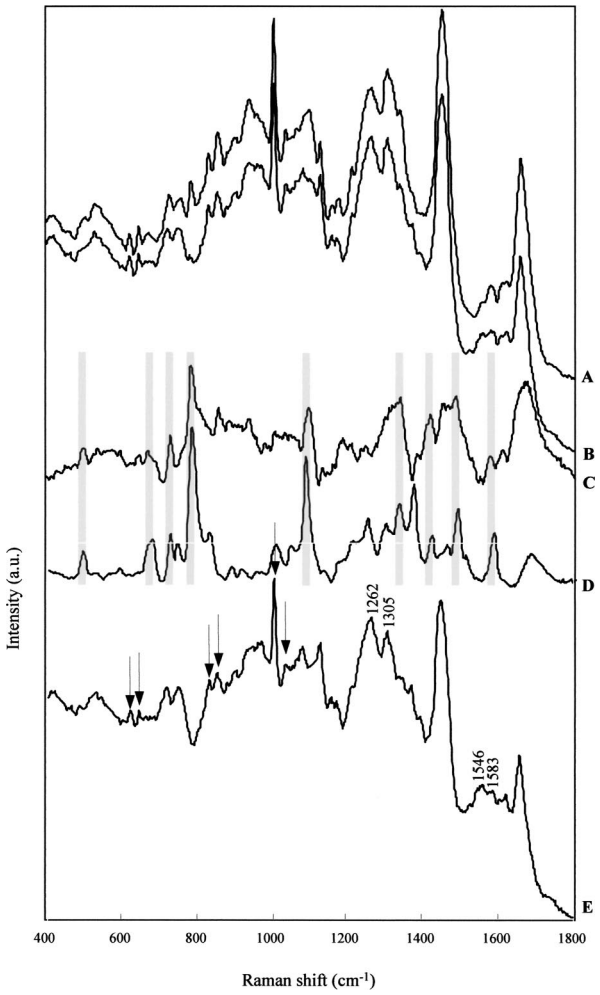

Fig. 4 Raman spectra obtained from the bronchial epithelium. A: average spectrum of nuclear epithelial cluster [cluster 1 in Fig. 2($\mathbf{B_3}$)]. B: average spectrum of cytoplasmic epithelial cluster [cluster 6 in Fig. 2($\mathbf{B_3}$)]. C: the difference spectrum between these two spectra (nuclear epithelial cluster minus cytoplasmic epithelial cluster) shows many spectral features (gray bars) of DNA. D: Raman spectrum of pure DNA. E: the difference spectrum cytoplasmic epithelial cluster minus nuclear epithelial cluster. The presence of protein signal contributions is suggested by spectral features of phenylalanine (621, 1004, and 1033 cm^{-1}) and tyrosine (644, 831, and 852 cm^{-1}), indicated by arrows. The prominent bands at 1262 and 1305 cm^{-1} imply the significant signal contributions of lipids in the cytoplasmic epithelial cluster. Furthermore, the Raman bands in the 1546 to 1583 cm^{-1} region are indicative of hemeproteins such as catalase.

3.2.3 *Submucosa*

Various spectral clusters were found in the submucosa, including those that represent groups of secreting glands and their ducts [Fig. 2($\mathbf{B_1}$), main clusters 10, 4, 12], fibrocollagenous stroma with smooth muscle bands [Fig. 2($\mathbf{B_1}$), clusters 7 and 8, respectively], and cartilage [Fig. 2($\mathbf{A_3}$), clusters 12 and 13].

Fibrocollagenous stroma. The differences in chemical composition of the main fibrocollagenous stroma cluster [cluster 7 of Fig. 2($\mathbf{B_1}$)] and smooth muscle bands [cluster 8 of Fig. 2($\mathbf{B_1}$)] were analyzed by means of a least-squares fit procedure (Fig. 5). Fibrocollagenous stroma contains a high concentration of collagen and smooth muscle contains a high concentration of actin and myosin.[23,24] Actin and myosin have similar Raman spectra.[26] The average spectrum of cluster 7 was fitted with the average spectrum of cluster 8 and the spectra of pure collagen and actin, which are shown as the fit spectra (spectra B, C, and D) after multiplication by the fit coefficients that resulted from the least-squares fit. Fit residual is shown in Fig. 5 spectrum E. Therefore a positive/negative spectrum signifies that more/less of that compound is present in cluster 7 than in cluster 8. It follows that in fibrocollagenous stroma, the concentration of collagen was higher and the concentration of actin was lower than in smooth muscle. For clarity, the spectra of pure collagen (spectrum F) and pure actin (spectrum G) are also shown.

Glands and gland ducts. Figure 6 displays a comparison of a cluster-averaged Raman spectrum obtained from the tissue layer lining the lumen of the glands and their ducts [spectrum A, cluster 12 in Fig. 2($\mathbf{B_1}$)] with spectrum of bronchial mucus at the epithelial surface and from gland duct [spectrum B, cluster 3 in Fig. 2($\mathbf{B_1}$)]. A high spectral resemblance is evi-

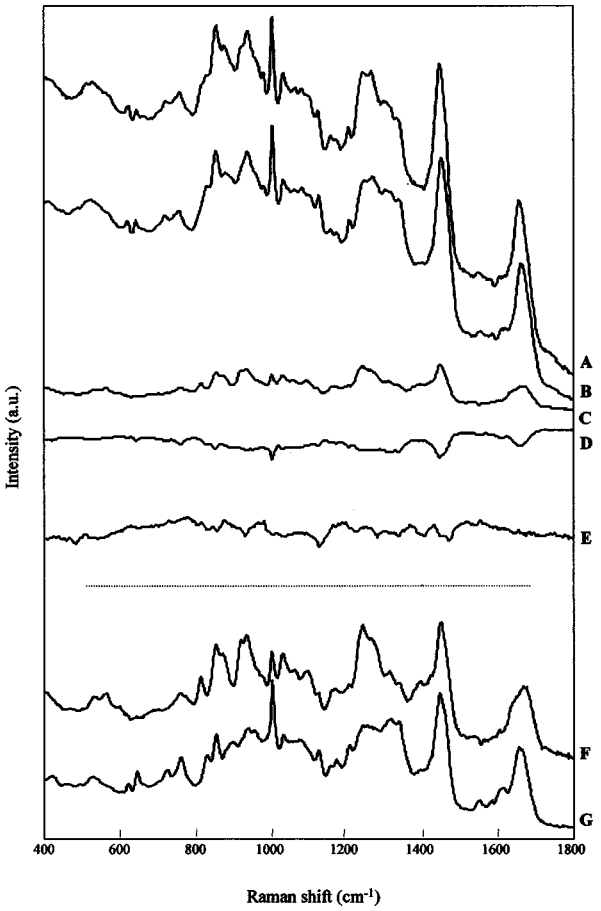

Fig. 5 The differences in chemical composition between fibrocollagenous stroma and smooth muscle analyzed by means of a least-squares fit procedure. The average spectrum of fibrocollagenous stroma [spectrum A, cluster 7 in Fig. 2(**B_1**)] was fitted with the average spectrum of smooth muscle [cluster 8 in Fig. 2(**B_1**)] and the spectra of pure collagen and pure actin. The fit spectra (spectra B, C, and D) are the average spectra of smooth muscle and of collagen and actin, respectively, which are shown after multiplication by the fit coefficients that resulted from the least-squares fit. The fit residual (spectrum E) suggests a higher collagen contribution and lower actin contribution in fibrocollagenous spectrum than in smooth muscle spectrum. For comparison with the fit spectra, the Raman spectra of pure collagen (spectrum F) and of pure actin (spectrum G) are also shown. For clarity of presentation, collagen spectrum was divided by factor 8 and actin spectrum by factor 10.

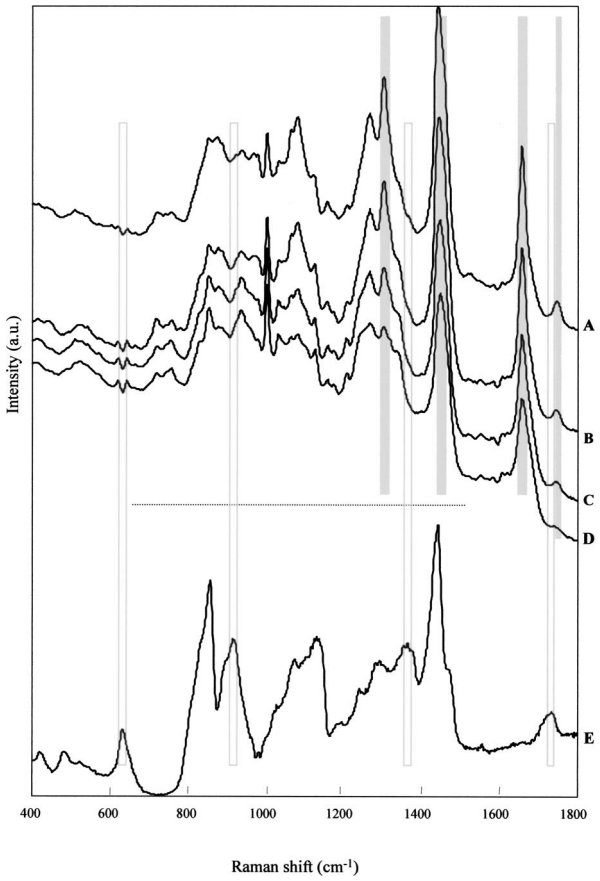

Fig. 6 Raman spectra obtained from bronchial mucus and from bronchial gland secretions. A: average spectrum obtained from bronchial mucus at the epithelial surface [cluster 3 in Fig. 2(**B_1**)]. B, C, and D: the cluster averages from the excretory gland duct, collected from the luminal surface toward the periphery of the duct [clusters 3, 4, and 10 respectively, in Fig. 2(**B_1**)]. There is a very high resemblance between spectra of bronchial mucus and spectra obtained from the tissue layer at the luminal side of the gland duct. Prominent Raman bands of lipids at 1301, 1440, 1656, and 1746 cm^{-1} (gray bars) show a decrease in signal from the luminal side of the duct toward its periphery. For comparison, spectrum obtained of pure Tissue Tek® is shown (E). Open bars highlight the absence of Tissue Tek® specific bands (at about 633, 916, 1364, and 1734 cm^{-1}) in the spectra shown in A to D.

dent. Raman spectra collected from the periphery of gland duct [spectra C and D, clusters 4 and 10 in Fig. 2(**B_1**)] are also shown. It is notable that there is a decrease in lipid signal contribution from the luminal side of the gland duct toward its periphery. Prominent Raman bands of lipids (gray bars) are present at 1301, 1440, 1656, and 1746 cm^{-1}. Furthermore, we have analyzed whether there was Tissue Tek® contamination of the spectra we have obtained. As displayed in Fig. 6 spectrum E (open bars), Raman spectrum of Tissue Tek® shows specific bands at 633, 916, 1364, and 1734 cm^{-1}, which do not contribute to the spectra recorded from bronchial mucus or from gland tissue. The tissue area captured in cluster 9 [Fig. 2(**B_1**)] demarcates a transition area between fibrocollagenous tissue and gland duct tissue. The spectrum of the transition area (Fig. 7 spectrum A) can be almost completely reconstructed from the spectrum of the fibrocollagenous stroma [cluster 7 of Fig. 2(**B_1**)] and the spectrum of the bronchial mucus on the epithelial surface [cluster 3 of Fig. 2(**B_1**)], as is evident from the very small fit-residual (Fig. 7 spectrum D). It suggests that some of the bronchial gland secretion diffuses into the fibrocollagenous tissue surrounding the ducts. The fit spectra (e.g., averaged spectra from fibrocollagenous stroma and from bronchial mucus) are shown after multiplication by the fit coefficients (Fig. 7 spectra B and C).

Cartilage. The Raman signal obtained from the cartilage [unstained tissue section; Fig. 2(**A_2**)] is shown in Fig. 8 (spectrum A). Significant Raman bands, which are mainly due to collagen (spectrum B), are highlighted (gray bars). Furthermore, Raman peaks at 413, 974, 1062, and 1337 cm^{-1} (arrows) suggest the presence of chondroitin sulfate,[27] which belongs to the group of sulfated glycosaminoglycans (GAGs).

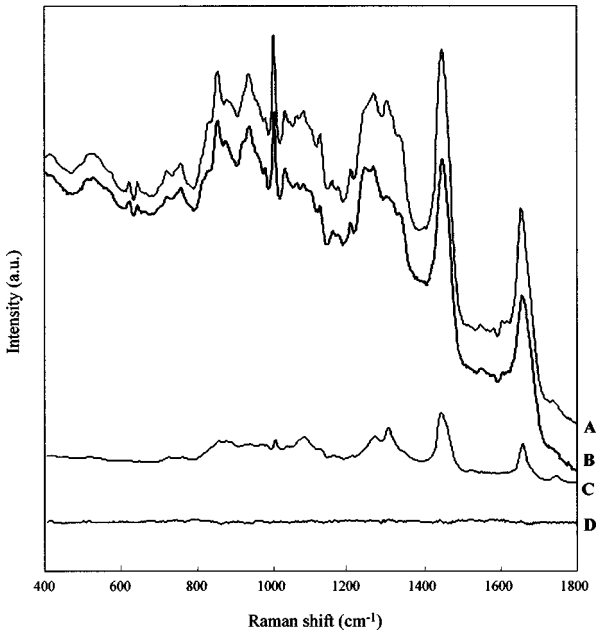

Fig. 7 Average spectrum of the tissue area [cluster 9 in Fig. 2($\mathbf{B_1}$)] between fibrocollagenous stroma and gland duct (A) was fitted with the average spectrum of fibrocollagenous stroma [cluster 7 of Fig. 2($\mathbf{B_1}$)] and the spectrum of bronchial mucus [cluster 3 of Fig. 2($\mathbf{B_1}$)]. The fit-spectra B and C are the average spectra of fibrocollagenous stroma and of bronchial mucus, respectively, which are shown after multiplication by the fit coefficients. The fit residual (D) implies that some of the secretion from the gland duct diffuses into the surrounding fibrocollagenous stroma.

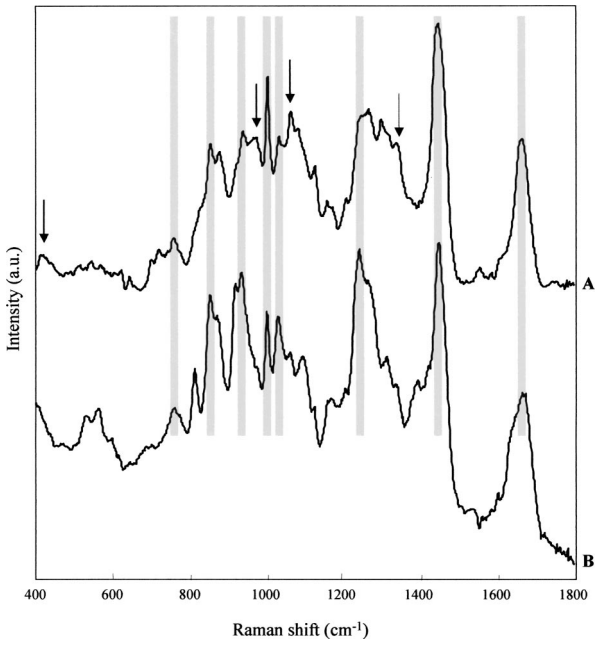

Fig. 8 Raman spectrum obtained from the bronchial wall cartilage. Comparison of Raman average spectrum of cartilage (spectrum A) with the spectrum of pure collagen (spectrum B). Spectral regions of the most prominent resemblance are highlighted by gray bars. For clarity of presentation, the collagen spectrum was divided by factor 6. Furthermore, the Raman bands visible at 413, 974, 1062, and 1337 cm^{-1} (arrows) can be assigned to sulfated glycosaminoglycans (GAGs) such as chondroitin sulfate.

(Note the strong band at 1062 cm^{-1}, which can be identified as the symmetric stretching vibration of the OSO_3^- group.[27])

4 Discussion

To date, only a few studies have addressed the lipid composition of bronchial mucus. Neutral lipids were the predominant lipids in normal airway secretions studied by Bhaskar et al.[28] In other studies, phospholipids represented the main content of bronchial mucus, and cholesterol was the principal neutral lipid.[29] Slomiany et al. reported that bronchial secretions consisted of similar quantities of neutral lipids and glycolipids.[30] Here we demonstrate that detailed analysis of Raman spectra (see Fig. 3) obtained from bronchial mucus reveals triolein as the major component of bronchial mucus. This is in line with studies describing neutral lipids as the primary compound of bronchial mucus. Furthermore, the Raman bands in the 1546 to 1583 cm^{-1} region (Fig. 4 spectrum E) are indicative of the presence of hemeproteins such as enzyme catalase in the cytoplasm of bronchial epithelial cells. This finding could be explained by secretion of antioxidants such as catalase by bronchial epithelium, to provide protection against potentially injurious agents.[24] In comparison with the nuclear epithelial cluster, higher lipid and protein signal contributions and lower DNA signal contributions (Fig. 4) were observed in the cytoplasmic epithelial cluster. As expected, collagen and actin/myosin were the major discriminators between fibrocollagenous stroma tissue and smooth muscle, although spectral features remain in the fit residual (Fig. 5 spectrum E). This is most probably due to the fact that aside from differences in collagen and actin concentration, these histological structures contain different amounts of a number of other compounds such as glycosaminoglycans, supportive cells (e.g., fibroblasts and fibrocits in fibrocollagenous stroma, myofibroblasts in smooth muscle), elastic fibers, and fat. Characteristic Raman spectra of cartilage, which is mainly composed of glycosaminoglycans (GAGs) that are associated with collagen fibers,[27] were also obtained.

Contradictory reports on the origin of lipids in the bronchial mucus have been published. In our study, a very high resemblance between the cluster-averaged Raman spectra obtained from the bronchial mucus at the epithelial surface and the luminal content of the glands and their ducts was found (Fig. 7). This implies that bronchial mucus is probably primarily produced by submucosal glands and transported to the epithelial surface via gland ducts. This is in line with reports claiming that the tracheobronchial mucus is mainly secreted by the airway secretory cells, although it may also contain some components from alveolar sources.[28,31,32] Some authors suggest the existence of conductive airway surfactant that has different biochemical and surface-tension properties compared to alveolar surfactant.[32,33]

We have studied tissue samples that were snap frozen directly after collection and performed the Raman analysis without any preceding processing (e.g., dies, labels). Although some artifacts were recognized [see Figs. 2($\mathbf{A_1}$) and 2($\mathbf{B_1}$)] that were due to the use of Tissue Tek® as an embedding agent (see Sec. 2 Materials and Methods), spectral analysis revealed that there was no spectral contamination, neither of the bronchial mucus nor of the tissue. This was very easy to

confirm, since Tissue Tek® specific bands were not present in the spectra we collected (Fig. 6 spectrum E, open bars). Other approaches to study the composition of bronchial lining secretion, like those on material obtained after laryngectomy or tracheotomy, tracheal aspirates, bronchopulmonary washings, sputum, surgically removed bronchogenic cysts, and secreting cell cultures are hampered by potential contamination of the sample by alveolar components or sputum.[32,34] In addition, sometimes only a fraction of the bronchial secretions was investigated (e.g., soluble phase only or fibrillar network only). It is clear that the uncertainty whether the sample that is being analyzed is actually representative of bronchial mucus is taken away by *in situ* analysis on unfixed tissues.

5 Concluding Remarks

In this study we analyze the Raman spectra obtained from snap frozen human bronchial tissue sections. Raman mapping experiments are performed and directly compared with the histology of the tissue sections. By precise linking of spectral features with the histologic structures, information about the (differences in) molecular composition of these structures is revealed. Hence, Raman spectroscopy may become an important tool in increasing our fundamental understanding of biological structures and their aberrations. A clear illustration of the power of such an approach is the straightforward way in which the main composition and source of the bronchial mucus could be analyzed. In various studies it was suggested that in diseases such as chronic bronchitis, asthma, and cystic fibrosis, the bronchial hypersecretion is accompanied by changes in biochemical composition of bronchial mucus.[22,29,31] Likewise, the presence of (pre-) malignant tissue may affect the formation and/or composition of the bronchial mucus. These are topics of continued research efforts in this area. In future *in vivo* measurements, most likely by means of fiber optics, the tissue volumes from which a signal will be obtained will be much larger than in this study. This implies that several different tissue layers and structures will contribute to the Raman signal that will be obtained. The detailed information obtained in this study is valuable for the interpretation of such spectra. With similar studies to be performed for pathologic conditions of bronchial tissue, such as malignancies and premalignant tissues, the development of *in vivo* diagnostic applications can be put on a solid basis.

References

1. S. Lam, T. Kennedy, M. Unger, Y. E. Miller, D. Gelmont, V. Rusch, B. Gipe, D. Howard, J. C. LeRiche, A. Coldman, and A. F. Gazdar, ''Localization of bronchial intraepithelial neoplastic lesions by fluorescence bronchoscopy,'' *Chest* **113**, 696–702 (1998).
2. B. J. Venmans, J. C. van der Linden, A. J. van Boxem, P. E. Postmus, E. F. Smit, and G. Sutedja, ''Early detection of pre-invasive lesions in high risk patients. A comparison of conventional fiberoptic and fluorescence bronchoscopy,'' *J. Bronchol.* **5**, 280–283 (1998).
3. Y. Kusunoki, F. Imamura, H. Uda, M. Mano, and T. Horai, ''Early detection of lung cancer with laser-induced fluorescence endoscopy and spectrofluorometry,'' *Chest* **118**, 1776–1782 (2000).
4. F. R. Hirsch, W. A. Franklin, and P. A. Bunn, ''Early detection of lung cancer: clinical perspectives of recent advances in biology and radiology,'' *Clin. Cancer Res.* **7**, 5–22 (2001).
5. F. R. Hirsch, S. A. Prindiville, Y. E. Miller, W. A. Franklin, E. C. Dempsey, J. R. Murphy, P. A. Bunn, Jr., and T. C. Kennedy, ''Fluorescence versus white-light bronchoscopy for detection of preneoplastic lesions: a randomized study,'' *J. Natl. Cancer Inst.* **93**, 1385–1391 (2001).
6. A. T. Tu, *Basic Concept and Elementary Theory: Raman Spectroscopy in Biology*, John Wiley and Sons, New York (1982).
7. G. J. Puppels, F. F. De Mull, C. Otto, J. Greve, D. J. Arndt-Jovin, and T. M. Jovin, ''Studying single living cells and chromosomes by confocal Raman microspectroscopy,'' *Nature (London)* **347**, 301–303 (1990).
8. A. Mahadevan-Jansen, M. F. Mitchell, N. Ramanujam, A. Malpica, S. Thomasen, U. Utzinger, and R. Richards-Kortum, ''Near-infrared Raman spectroscopy for in vitro detection of cervical precancers,'' *Photochem. Photobiol.* **68**, 123–132 (1998).
9. E. B. Hanlon, R. Manorahan, T. W. Koo, K. E. Shafer, J. T. Motz, M. Fitzmaurice, L. R. Kramer, I. Itzakan, R. R. Dasari, and M. S. Feld, ''Prospects for in vivo Raman spectroscopy,'' *Phys. Med. Biol.* **45**, R1–R59 (2000).
10. T. C. Bakker Schut, M. Witjes, M. Sterenborg, O. Speelman, J. Roodenburg, E. Marple, H. A. Bruining, and G. J. Puppels, ''In vivo detection of dysplastic tissue by Raman spectroscopy,'' *Anal. Chem.* **72**, 6010–6018 (2002).
11. A. Nijssen, T. C. Bakker Schut, F. Heule, P. J. Caspers, D. P. Hayes, M. H. A. Neumann, and G. J. Puppels, ''Discriminating basal cell carcinoma from its surrounding tissue by Raman spectroscopy,'' *J. Invest. Dermatol.* **119**, 64–69 (2002).
12. S. Koljenović, L. P. Choo-Smith, T. C. Bakker Schut, J. M. Kros, H. J. van den Berge, and G. J. Puppels, ''Discriminating vital tumor from necrotic tissue in human glioblastoma tissue samples by Raman spectroscopy,'' *Lab. Invest.* **82**, 1265–1277 (2002).
13. N. N. Boustany, J. M. Crawford, R. Manoharan, R. R. Dasari, and M. S. Feld, ''Analysis of nucleotides and aromatic amino acids in normal and neoplastic colon mucosa by ultraviolet resonance Raman spectroscopy,'' *Lab. Invest.* **79**, 1201–1214 (1999).
14. S. Kaminaka, T. Ito, H. Yamazaki, E. Kohda, and H. Hamaguchi, ''Near-infrared multichannel Raman spectroscopy toward real-time in vivo cancer diagnosis,'' *J. Raman Spectrosc.* **33**, 498–502 (2002).
15. R. Buschman, E. T. Marple, M. L. Wach, B. Bennett, T. C. Bakker Schut, H. A. Bruining, A. V. Bruschke, A. van der Laarse, and G. P. Puppels, ''In vivo determination of the molecular composition of artery wall by intravascular Raman spectroscopy,'' *Anal. Chem.* **72**, 3771–3775 (2000).
16. U. Utzinger, D. L. Heintzelman, A. Mahadevan-Jansen, A. Malpica, M. Follen, and R. Richards-Kortum, ''Near-infrared Raman spectroscopy for detection of cervical precancers,'' *Appl. Spectrosc.* **55**, 955–959 (2001).
17. S. W. E. van de Poll, T. J. Romer, O. L. Volger, D. J. M. Delsing, T. C. Bakker Schut, H. M. G. Princen, J. W. Jukema, L. Havekes, A. van der Laarse, and G. J. Puppels, ''Raman spectroscopic evaluation of the effects of diet and lipid-lowering therapy on athertosclerotic plaque development in mice,'' *Arterioscler., Thromb., Vasc. Biol.* **21**, 1630–1635 (2001).
18. R. Wolthuis, T. C. Bakker Schut, P. J. Caspers, H. P. Buschman, T. J. Römer, H. A. Bruining, and G. J. Puppels, ''Raman spectroscopic methods for in vitro and in vivo tissue characterization,'' Chap. 32 in *Fluorescent and Luminescent Probes for Biological Activity*, Mason, W. T., Ed., pp. 433–455, Academic Press, San Diego, CA (1999).
19. I. T. Jollife, *Principal Component Analysis*, Springer-Verlag, New York (1986).
20. A. K. Jain and R. C. Dubes, *Algorithms for Clustering Data*, Prentice Hall, Engelwood Cliffs, NJ (1988).
21. G. J. Puppels, H. S. P. Garritsen, J. A. Kummer, and J. Greve, ''Carotenoids located in human lymphocyte subpopulations and natural killer cells by Raman microspectroscopy,'' *Cytometry* **14**, 251–256 (1993).
22. J. H. Widdicombe and J. G. Widdicombe, ''Regulation of human airway surface liquid,'' *Respir. Physiol.* **99**, 3–12 (1995).
23. A. Stevens and J. Lowe, *Human Histology*, Times Mirror International Publishers Limited, London (1997).
24. V. H. J. van der Velden, H. F. J. Savelkoul, and M. A. Versnel, ''Bronchial epithelium: morphology, function, and pathophysiology in asthma,'' *European Cytokine Network* **9**, 585–598 (1998).
25. E. W. Blanch, L. A. Morozova-Roche, L. Hecht, W. Noppe, and L. D. Barron, ''Raman optical activity characterisation of native and molten globule states of equine lysozyme: comparison with hen lysozyme and bovine α-lactalbumin,'' *Biopolymers* **57**, 235–248 (2000).
26. E. B. Carew, H. E. Stanley, J. C. Seidel, and J. Gergely, ''Studies of

myosin and its proteolytic fragments by laser Raman spectroscopy,'' *Biophys. J.* **44**, 219–224 (1983).
27. R. Bansil, I. V. Yannas, and H. E. Stanley, ''Raman spectroscopy: a structural probe of glycosaminoglycans,'' *Biochim. Biophys. Acta* **541**, 535–542 (1978).
28. K. R. Bhaskar, D. D. O'Sullivan, J. Seltzer, T. H. Rossing, J. M. Drazen, and L. M. Reid, ''Density gradient study of bronchial mucus aspirates from healthy volunteers (smokers and non-smokers) and from patients with tracheostomy,'' *Exp. Lung Res.* **9**, 289–308 (1985).
29. K. C. Kim, H. Opaskar-Hincman, and K. R. Bhaskar, ''Secretions from primary hamster tracheal surface epithelial cells in culture: mucine-like glycoproteins, proteoglycans, and lipids,'' *Exp. Lung Res.* **15**, 299–314 (1989).
30. A. Slomiany, V. L. N. Murty, M. Aono, C. E. Snyder, A. Herp, and B. L. Slomiany, ''Lipid composition of tracheobronchial secretions from normal individuals and patients with cystic fibrosis,'' *Biochim. Biophys. Acta* **710**, 106–111 (1982).
31. L. M. Reid and K. R. Bhaskar, ''Macromolecular and lipid constituents of bronchial epithelial mucus,'' *Symp. Soc. Exp. Biol.* **43**, 201–219 (1986).
32. J. G. Widdicombe, ''Role of lipids in airway function,'' *Eur. J. Respir. Dis.* **71**, 197–204 (1987).
33. S. Girod, C. Fuchey, C. Galabert, S. Lebonvallet, N. Bonnet, D. Ploton, and E. Puchelle, ''Identification of phospholipids in secretory granules of human submucosal gland respiratory cells,'' *J. Histochem. Cytochem.* **39**, 193–198 (1991).
34. P. Roussel, P. Degand, G. Lamblin, A. Laine, and J. J. Lafitte, ''Biochemical definition of human tracheobronchial mucus,'' *Lung* **154**, 241–260 (1978).